Incorporation of a Variational Registration Method into a Spectroscopy Tool

Juan José Fuertes[1], Valery Naranjo[1], Rafael Verdú-Monedero[2], Ángela Bernabeu[3], Fernando López-Mir[1], Jorge Larrey-Ruiz[2], Juan Morales-Sánchez[2], Javier Sánchez[4] and Mariano Alcañiz[1,5]

[1]Instituto Interuniversitario de Investigación en Bioingeniería y Tecnología Orientada al Ser Humano, Universitat Politècnica de València, I3BH/LabHuman, Camino de Vera s/n, 46022 Valencia, Spain
[2]Universidad Politécnica de Cartagena, Cartagena, 30202, Spain
[3]Inscanner S.L., Unidad de Resonancia Magnética
[4]Philips Healthcare España, María de Portugal 1, 28050 Madrid, Spain
[5]Ciber, Fisiopatología de Obesidad y Nutrición, CB06/03 Instituto de Salud Carlos III, Spain
jjfuertes@labhuman.i3bh.es www.labhuman.com

Abstract. This work describes the incorporation of a variational image registration algorithm into an interactive medical tool to support clinical decision about treatment of brain pathologies. Through the combination of anatomical (Magnetic Resonance Images, MRI), functional (Positron Emission Tomography, PET) and molecular images (Chemical Shift Imaging, CSI) clinicians can determine the best therapeutic strategy in every case. First, MRI images and CSI are co-registered and analysed in order to create colour maps related with the concentration of metabolites in the brain. Then, PET and MRI are also registered since it allows knowing the metabolic functionality of the brain. The improvement of the Correlation Ratio (CR), the Structural SIMilarity (SSIM) and the Mutual Information (MI) shows the performance of the variational registration method which is at least two times faster than other approaches in the spatial domain. The goal of this tool is to provide surgeons as much information as possible to perform biopsies and/or surgeries.

Keywords: Magnetic resonance imaging, Positron emission tomography, Chemical shift imaging, Variational image registration, Multivoxel spectroscopy.

1 Introduction

Magnetic Resonance Imaging (MRI) of the human brain includes anatomical description and lesions detection, being the procedure of choice for most of the brain disorders. It provides high-resolution anatomical images of the brain which are difficult to obtain on a Computed Tomography (CT) scan. It is also useful

for the diagnosis of brain tumours and demyelinating disorders such as and multiple sclerosis (MS) that causes destruction of the myelin sheath of the nerve [1]. However, sometimes clinicians do not know if a specific area is harmful or not. In this context Chemical Shift Imaging (CSI), also known as multi-voxel Magnetic Resonance Spectroscopy (MRS), plays an important role providing additional metabolic information when a pathology is characterized. CSI is mainly used for tissue metabolism studies and tumour types differentiation [2]. The data acquired with CSI technique are presented as a spectrum, consisting of a group of graphs showing the relation between signal intensity and proton resonance frequency. If these spectra are processed and the area under the curve or the amplitude ratios between the brain metabolites are calculated, a colour map can be created and overload to the corresponding anatomical image. In this way, MRS provides additional biochemical information to the anatomical information, helping medical doctors in the characterization, diagnosis and management of several brain pathologies. During the last 20 years, many spectroscopic tools have been developed to solve the problem of quantifying signals in ^{1}H MRS data, highlighting among a large series of different software applications the jMRUI software package [3], the LCModelTM [4] and the AQSES software [5] among a large series of software applications. All of them incorporate the main algorithms to process the spectroscopic signals and generate the metabolite maps over the MR images. However, none of them integrate within the tool other kinds of images in order to complement the information which CSI gives to clinicians. Fuertes et al. [6] showed a multi-voxel MR spectroscopy tool for brain pathology detection, where the colour maps could be easily generated. In order to increase the software functionalities, the incorporation of a non-rigid image registration algorithm into the tool is presented in this paper, with the purpose of incorporating Positron Emission Tomography (PET) images into the tool improving pathologies detection. PET scans, with the use of a short-lived radioactive tracer isotope which is injected into the living subject, can often find changes in the body's tissues before changes can be seen in their structure, using a short-lived radioactive tracer isotope which is injected into the living subject [7]. At that point, the goal of this paper is to present the incorporation of an efficient algorithm into the tool that allows the clinicians to work with three different types of images, getting the most important features of each one. The method is based on an efficient implementation in the frequency domain of variational image registration, which is at least two times faster than other approaches in the spatial domain [8].

2 Software Tool

The software we introduce, also known as IMFUTEC [6] (see Figure 1), incorporates the main algorithms to process spectroscopy signals and performs a rigid registration between metabolite maps generated by means of spectroscopic data analyses and MRI images. It combines the effects of molecular distribution on the magnetic field experienced by an atomic nucleus, the Chemical Shift

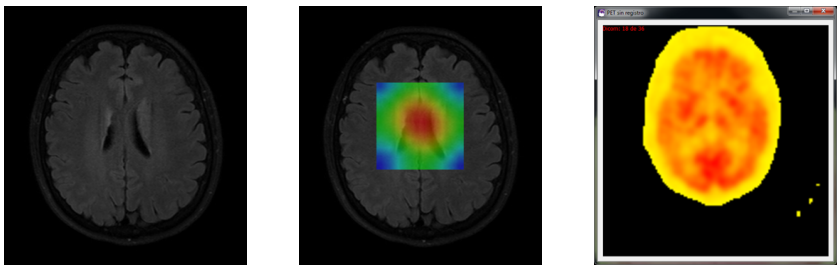

(a) (b) (c)

Fig. 1: Medical Imaging Modalities in IMFUTEC: (a) MRI, (b) CSI, (c) PET.

Imaging, with the effects of the magnetic field gradients used in MRI. Once the registration algorithm was incorporated, they will be combined with the effects of the positron emitters used in PET. The registration unit is divided mainly in two blocks: in the first, anatomical images are registered with the spectra data (rigid registration) to select the voxel signals which are processed to generate the metabolite maps. In the second block, the functional and anatomical images are registered (non-rigid registration) thanks to the incorporation of the variational registration algorithm.

2.1 Rigid registration between MRI and CSI

The first step for rigid image registration is to locate both anatomical and spectroscopic images in the 2D/3D space with their own rotation matrix. The whole spectroscopy imaging has a size of $H * W * P$ millimetres, where H stands for height, W stands for width and P stands for depth. In this way, the size of each spectroscopy slice and voxel can be calculated. The whole anatomical imaging has a size of $H * W * P$ millimetres, where H also stands for height, W for width and P for depth. At this point, it is possible to know which anatomical images belong to each spectroscopic image, through the expression:

$$e(\mathbf{x}, \mathbf{y}, \mathbf{z}) = c(\mathbf{x}, \mathbf{y}, \mathbf{z}) + t * M'. \tag{1}$$

where the absolute position of each spectroscopic slice is calculated. $e(\mathbf{x}, \mathbf{y}, \mathbf{z})$ is the absolute position of the edges of the spectrum, $c(\mathbf{x}, \mathbf{y}, \mathbf{z})$ is the center of the Field Of View (FOV), t is the thickness of each slice and M is the rotation matrix. Figure 2 shows the main window where we can see the anatomical images with the spectroscopic voxels. The red box belongs to the FOV of the spectroscopy imaging and the green box belongs to the area of those voxels which are excited, (Volume Of Interest, VOI).

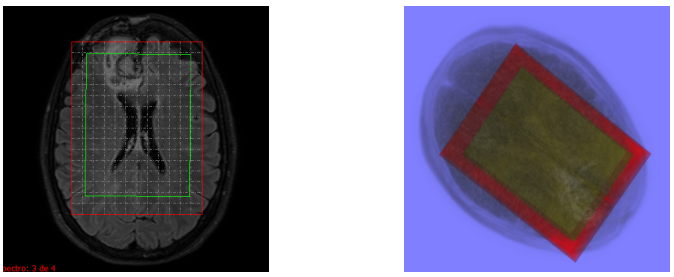

(a) (b)

Fig. 2: MRI-CSI registration:(a)FOV and VOI over anatomical image, (b) MRI-CSI 3D view.

3 Variational image registration between MRI and PET

Image registration is the process of finding out the global and local correspondence between two images, template T and reference R, of a scene in such a way that the transformed template and reference match [9]. For many years, researchers have developed and implemented registration algorithms for medical imaging applications, being non-rigid registration the most used method [10].

In this application the images are 3D datasets obtained from MRI and PET studies, $R, T : \mathbb{R}^3 \to \mathbb{R}$, and the registration will produce a non-rigid displacement field $\mathbf{u} : \mathbb{R}^3 \to \mathbb{R}^3$ that will make the transformed template dataset similar to the reference dataset, $T(\mathbf{x} - \mathbf{u}(\mathbf{x})) \approx R(\mathbf{x})$, where $\mathbf{u}(\mathbf{x}) = (u_1(\mathbf{x}), u_2(\mathbf{x}), u_3(\mathbf{x}))^\top$ and $\mathbf{x}$ is the spatial position $\mathbf{x} = (x_1, x_2, x_3) \in \mathbb{R}^3$. The non-parametric registration can be approached in terms of the variational calculus, by defining the joint energy functional to be minimized:

$$\mathcal{J}[\mathbf{u}] = \mathcal{D}[R, T; \mathbf{u}] + \alpha \mathcal{S}[\mathbf{u}]. \tag{2}$$

The energy term $\mathcal{D}$ measures the distance between the deformed template dataset and the reference dataset; $\mathcal{S}$ is a penalty term which acts as a regularizer and determines the smoothness of the displacement field; and $\alpha > 0$ weights the influence of the regularization. The distance measure $\mathcal{D}$ is chosen depending on the datasets to be registered. When dealing with datasets from different sources or modalities (multimodal registration), statistical-based measures are more appropriate. In this application the correlation ratio [11] has been used. The regularization term $\mathcal{S}$ gives the smoothness characteristics to the displacement field [12]. In our case we use the diffusion term, which is given by the energy of first order derivatives of $\mathbf{u}$:

$$\mathcal{S}^{\text{diff}}[\mathbf{u}] = \frac{1}{2} \sum_{l=1}^{3} \int_{\mathbb{R}^3} \|\nabla u_l\|^2 \, d\mathbf{x}. \tag{3}$$

As described in [13], the joint energy functional (2) can be translated into the frequency domain by means of Parseval's theorem, then $\mathcal{J}[\mathbf{u}] = \tilde{\mathcal{J}}[\tilde{\mathbf{u}}]$, where

$$\tilde{\mathcal{J}}[\tilde{\mathbf{u}}] = \tilde{\mathcal{D}}[\tilde{R}, \tilde{T}; \tilde{\mathbf{u}}] + \alpha\, \tilde{\mathcal{S}}[\tilde{\mathbf{u}}], \tag{4}$$

with $\tilde{\mathbf{u}}(\boldsymbol{\omega}) = (\tilde{u}_1(\boldsymbol{\omega}), \tilde{u}_2(\boldsymbol{\omega}), \tilde{u}_3(\boldsymbol{\omega}))^\top$ being the frequency counterpart of the displacement field, $\boldsymbol{\omega} = (\omega_1, \omega_2, \omega_3)$ is the three dimensional variable in the frequency domain,

According to the variational calculus, a necessary condition for a minimizer $\tilde{\mathbf{u}}$ of the joint energy functional (4) is that the first variation of $\tilde{\mathcal{J}}[\tilde{\mathbf{u}}]$ in any direction (also known as the *Gâteaux* derivative) vanishes for all suitable perturbations. This leads to the Euler-Lagrange equation in the frequency domain:

$$\tilde{\mathbf{f}}(\boldsymbol{\omega}) + \alpha\, \tilde{\mathcal{A}}(\boldsymbol{\omega})\, \tilde{\mathbf{u}}(\boldsymbol{\omega}) = \mathbf{0}, \tag{5}$$

where $\tilde{\mathbf{f}}$ is the 3D Fourier transform of the external forces, $\mathcal{FT}\{\nabla \mathcal{D}[R, T; \mathbf{u}]\}$, and $\tilde{\mathcal{A}}$ is a diagonal 3×3 matrix whose elements are scalar functions which implement the spatial derivatives in the frequency domain, allowing for their computation by means of products:

$$\tilde{\mathcal{A}}_{ii}(\boldsymbol{\omega}) = 2 \sum_{m=1}^{3} (1 - \cos \omega_m)\,. \tag{6}$$

The Euler-Lagrange equations (5) in the frequency domain provide a stable implementation for the computation of a numerical solution for the displacement field, and in a more efficient way than existing approaches if the three-dimensional fast Fourier transform is used. To solve (5), formulated in the frequency domain, a time-marching scheme can be employed, yielding the following equation:

$$\partial_t \tilde{\mathbf{u}}(\boldsymbol{\omega}, t) + \tilde{\mathbf{f}}(\boldsymbol{\omega}, t) + \alpha\, \tilde{\mathcal{A}}(\boldsymbol{\omega})\, \tilde{\mathbf{u}}(\boldsymbol{\omega}, t) = \mathbf{0}, \tag{7}$$

where $\partial_t \tilde{\mathbf{u}}(\boldsymbol{\omega}, t) = (\partial_t \tilde{u}_1(\boldsymbol{\omega}, t), \partial_t \tilde{u}_2(\boldsymbol{\omega}, t), \partial_t \tilde{u}_3(\boldsymbol{\omega}, t))^\top$ (in the steady-state $\partial_t \tilde{\mathbf{u}}(\boldsymbol{\omega}, t) = \mathbf{0}$ and (7) holds (5)). Equation (7) is solved by discretizing the time, $t = \xi\tau$, $\tau > 0$ being the time-step and $\xi \in \mathbb{N}$ being the iteration index, and the time derivative of $\tilde{\mathbf{u}}(\boldsymbol{\omega}, t)$ is replaced by the first backward difference. Using the notation $\tilde{\mathbf{u}}^{(\xi)}(\boldsymbol{\omega}) = \tilde{\mathbf{u}}(\boldsymbol{\omega}, \xi\tau)$, the following semi-implicit iterative scheme comes out:

$$\tilde{u}_l^{(\xi)}(\boldsymbol{\omega}) = H(\boldsymbol{\omega})\big(\tilde{u}_l^{(\xi-1)}(\boldsymbol{\omega}) - \eta^{-1}\, \tilde{f}_l^{(\xi-1)}(\boldsymbol{\omega})\big), \tag{8}$$

where $l = \{1, 2, 3\}$, $\eta = 1/\tau$ and $H(\boldsymbol{\omega})$ is the following 3D low pass filter $H(\boldsymbol{\omega}) = (1 + \eta^{-1}\alpha \tilde{\mathcal{A}}_{ii}(\boldsymbol{\omega}))^{-1}$. An implementation based on the 3D FFT is, in terms of efficiency, two times faster than the fastest implementation available in the spatial domain [8], which is the DCT-based algorithm included in the FLIRT toolbox [12] for the diffusion and curvature registration methods [14].

4 Registration Results

This section shows the non-rigid alignment between different MRI datasets and a PET dataset acquired in two different scanners. The MRI datasets are FFE (Fast Field Echo), FLAIR (Fluid Attenuated Inversion Recovery) and TSE (Turbo Spin Echo) resonance images of the same patient acquired at different times. The studies were obtained using a Philips 3T Achieva scanner for MRI, and a Siemens PET/CT 16 scanner for PET, being the images reformatted into DICOM files of different resolutions. For all experiments shown in this work, the used registration parameters were: $\eta = 1$, $\alpha = 200$ and the maximum number of iterations $\xi_{max} = 250$. With these parameters, the optimal performance of the algorithm is achieved, obtaining at the same time a likely and smooth transformation. The diffusion regularizer $\mathcal{S}^{\text{diff}}$ ensures a correct outcome in this scenario since it privileges translations in the computed displacement field $\mathbf{u}$ [15]. The following figures and tables shown the performance of the non-rigid registration algorithm: the results are satisfactory both visually and numerically, since PET and MRI registration has been validated by an experienced clinician. Fig. 3 displays the registration of a FFE volume resonance (reference dataset, R) and a PET volume (template dataset, T) of the same patient. In the second experiment, (Figure 4) the aim was to register FLAIR resonances (reference dataset, R) and PET (template dataset, T). The last experiment displayed in Figure 5, shows the registration of the TSE (reference dataset, R) and PET volumes(template dataset, T). The outcome of the proposed registration algorithm is shown in the second column of Figure 5. Table 1 gathers the similarities measurements in terms of Correlation Ratio (CR) [11], Structural Similarity (SSIM) [16] and Mutual Information (MI) [17] regardless of the kind of resonance image: promising results are achieved since CR, SSIM and MI parameters improve after registering. Future experiments will focus on registering MRI and TAC volumes and consequently, PET images, comparing both experiments. Figure 6 shows in red-hot scale the performance of the algorithm after registering MRI and PET images in the IMFUTEC tool. It is also displayed the CSI colour map over the MR image in order to provide surgeons as much information as possible.

Table 1: Similarity measures computed for the registration of PET-FLAIR, PET-FFE and PET-TSE volumes.

PET-FLAIR	CR	SSIM	MI
Before registration	40.99%	0.405	0.4721 bits
After registration	72.21%	0.493	0.8749 bits
PET-FFE			
Before registration	51.83%	0.665	0.5436 bits
After registration	87.90%	0.819	1.0526 bits
PET-TSE			
Before registration	41.69%	0.560	0.4938 bits
After registration	76.18%	0.771	1.0468 bits

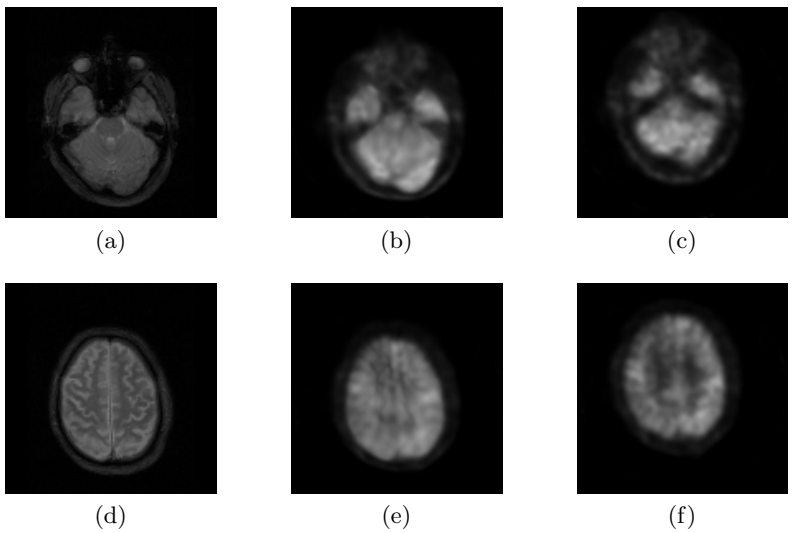

Fig. 3: Registration of PET and FFE volumes of the same patient ($128 \times 128 \times 64$ voxels). First column: reference dataset. Second column: registered template. Third column: template dataset. First row: slice #16. Second row: slice #48.

5 Conclusions and Future Work

This work describes the incorporation of a variational image registration algorithm into an interactive medical tool to support clinical decision about treatment of brain pathologies. Thus, the software lets surgeons decide the better strategy to diagnose and treat the brain pathology through the use of Magnetic Resonance Spectroscopy (anatomical), Chemical Shift Imaging (molecular) and Positron Emission Tomography (functional information). Thanks to the incorporation of a variational image registration algorithm into the medical tool, it is possible to register different types of medical images in order to support clinical decision about treatment of brain pathologies. Both numerical and visual results show the performance of the algorithm, being that results validated by an experienced clinician. In this way, the final application integrates those algorithms that are daily used in spectroscopy tools, providing the clinician with a user-friendly tool and with the information of the three types of imaging. Coming soon experiments will be focused on placing together the information of MRI, PET and CSI into an Automated Decision Support System for the detection of brain pathologies. As far as new tool methods are concerned, the registration and fusion with other kinds of images such as Diffusion Tensor Imaging (DTI) and functional Magnetic Resonance (fMRI) are being studied. The goal is to unify the information from different types of medical images to perform a 3D full brain image reconstruction.

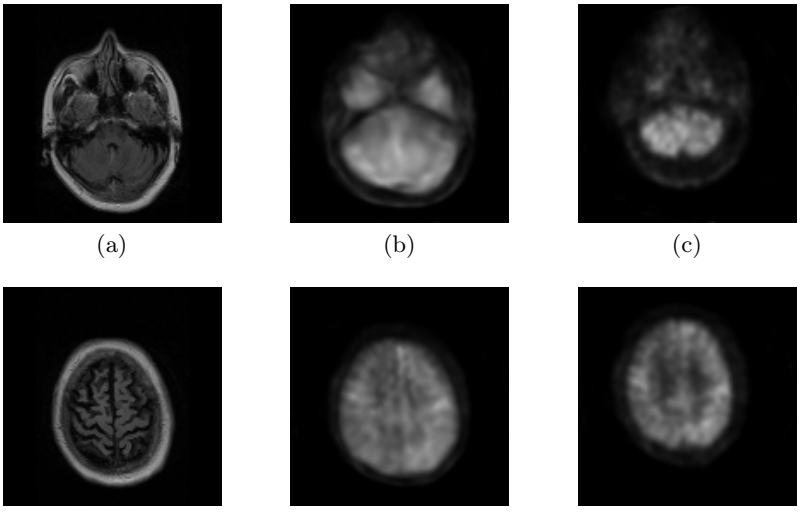

Fig. 4: Registration of PET and FLAIR volumes of the same patient ($128 \times 128 \times 64$ voxels). First column: reference dataset. Second column: registered template. Third column: template dataset. First row: slice #12. Second row: slice #48.

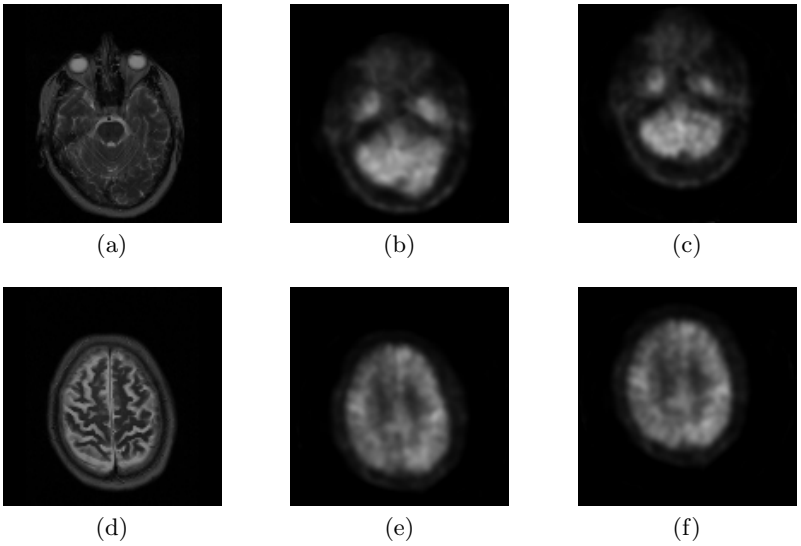

Fig. 5: Registration of PET and TSE volumnes of the same patient ($128 \times 128 \times 64$ voxels). First column: reference dataset. Second column: registered template. Third column: template dataset. First row: slice #14. Second row: slice #48.

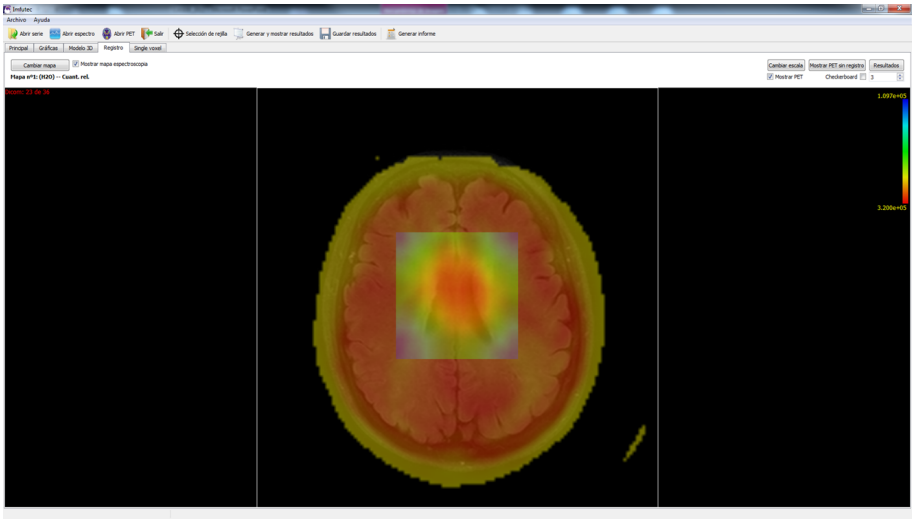

Fig. 6: MRI-CSI-PET registration in IMFUTEC

Acknowledgements

This work has been supported by Centro para el Desarrollo Tecnológico Industrial (CDTI) under the project ONCOTIC (IDI-20101153), and partially by projects Consolider-C (SEJ2006-14301/PSIC), CIBER of Physiopathology of Obesity and Nutrition, an initiative of ISCIII and Excellence Research Program PROMETEO (Generalitat Valenciana. Consellería de Educación, 2008-157). We would like to express our deep gratitude to the Hospital Clínica Benidorm for its participation in this project. The work of Juan José Fuertes has been supported by a FPI grant from Programa de Ayudas de Investigación y Desarrollo (PAID) of UPV.

References

1. Bushong, S.C.: Magnetic Resonance Imaging: Physical and Biological Principles, 3e. Mosby, 3rd edition (2003).
2. Castillo, M., K.L. and Mukherji, S.: Clinical application of proton mr spectroscopy. American Journal of Neuroradiology, 17:1–15 (1996).
3. Stefan, D., Cesare, F. D., Andrasescu, A., Popa, E., Lazariev, A., Vescovo, E., Strbak, O., Williams, S., Starcuk, Z., Cabanas, M., van Ormondt, D., and Graveron-Demilly, D.: Quantitation of magnetic resonance spectroscopy signals: the jmrui software package. Measurement Science and Technology, 20(10):104035 (2009).
4. Gruber, S., S. A. M. V. G. O. and Moser, E.: An lcmodel-based automatic software tool for the reconstruction of anatomically- and pathologically-matched voxels using high-resolution 3d-spectroscopic imaging: Applications in tumour patients. In Proceedings of the ISMRM 12th Annual Meeting, 11 (2004).

5. Simonetti, A., Poullet, J.-B., Sima, D., De Neuter, B., Vanhamme, L., Lemmerling, P., and Van Huffel, S.: An open source short echo time MR quantitation software solution: AQSES. Technical Report 05-168, ESAT-SISTA, K.U. Leuven (2006).
6. Fuertes, J. J., Naranjo, V., González, P., Bernabeu, Á., Raya, M. A., and Sanchez, J.: Multivoxel mr spectroscopy tool for brain cancer detection in neuronavigation performance. In BIODEVICES, 167–172 (2012).
7. Chen, W.: Clinical applications of pet in brain tumors. Journal of nuclear medicine official publication Society of Nuclear Medicine, 48(9):1468–1481 (2007).
8. Verdu-Monedero, R., Larrey-Ruiz, J., and Morales-Sanchez, J.: Frequency implementation of the euler-lagrange equations for variational image registration. Signal Processing Letters, IEEE, 15:321–324(2008).
9. Zitová, B. and Flusser, J.: Image registration methods: a survey. Image and Vision Computing, 21:977–1000 (2003).
10. D'Agostino, E., Maes, F., Vandermeulen, D., and Suetens, P.: A Viscous Fluid Model for Multimodal Non-rigid Image Registration Using Mutual Information.In Medical Image Computing and Computer-Assisted Intervention - MICCAI 2002, 541–548 (2002).
11. Roche, A., Malandain, G., Pennec, X., and Ayache, N.: The correlation ratio as a new similarity measure for multimodal image registration. 1115–1124. Springer Verlag (1998).
12. Fischer, B. and Modersitzki, J.: Flirt: A flexible image registration toolbox. In Biomedical Image Registration: Second International Workshop, WBIR 2003, 261–270. Springer-Verlag (2003).
13. Larrey-Ruiz, J., Monedero, R. V., and Morales-Sánchez, J.: A fourier domain framework for variational image registration. Journal of Mathematical Imaging and Vision, 32(1):57–72 (2008).
14. Haber, E. and Modersitzki, J.: Numerical methods for image registration (2004).
15. Modersitzki, J.: Numerical Methods for Image Registration. Oxford University Press, USA (2004).
16. Wang, Z., Bovik, A., Sheikh, H., and Simoncelli, E.: Image quality assessment: from error visibility to structural similarity. Image Processing, IEEE Transactions on, 13(4):600–612 (2004).
17. Maes, F., Vandermeulen, D., and Suetens, P.: Medical image registration using mutual information. Proceedings of the IEEE, 91(10):1699–1722 (2003).